



Contents lists available at ScienceDirect

## Journal of Quantitative Spectroscopy &amp; Radiative Transfer

journal homepage: [www.elsevier.com/locate/jqsrt](http://www.elsevier.com/locate/jqsrt)

## Notes

## Leaf scattering polarimetry and chlorophyll fluorescence

W.E. Martin



Centre for Astrophysics Research and Centre for Atmospheric and Climate Physics Research, University of Hertfordshire, UK

## ARTICLE INFO

## Article history:

Received 7 October 2019

Revised 15 November 2019

Accepted 15 November 2019

Available online 16 November 2019

## ABSTRACT

A number of spectropolarimetry measurements on leaves using white light and narrow band illumination have been reported in recent years because of interest in signatures for remote sensing of exoplanet life. Chlorophyll fluorescence occurs in white light illuminated experiments and is known to be polarised and so might contaminate surface scattering measurements. A displacing filter experiment was performed on the leaves of two common plants, *Ficus benjamina* and *Chamaedorea elegans*, to estimate the contribution of chlorophyll fluorescence in the spectropolarimetry of leaf scattering and transmission. Chlorophyll fluorescence is present as a measurable polarised component of up to 15% of scattered and transmitted light for the leaf samples. Other effects emerged which indicate that in vivo measurements on leaves are subject to the responsive nature of the leaves to changes in colour and intensity of the incident light.

Crown Copyright © 2019 Published by Elsevier Ltd.

This is an open access article under the CC BY license. (<http://creativecommons.org/licenses/by/4.0/>)

## 1. Background

Spectropolarimetry has been used to explore linear and circular polarised scattering from a variety of algae and plant leaves to measure possible chiral scattering effects that could potentially be used to identify the presence of photosynthesis in the optical signature of exoplanets [1–6]. There are a number of persistent issues amongst the current measurements including the large variety of plants and algae used by various experimenters, the lack of agreed standards, and differing techniques and apparatus to measure nominally the same set of Stokes and Mueller matrix components of the scattered or transmitted light. This short article attempts to address one aspect of the comparison of spectropolarimetric experiments with one another, namely the presence of polarised fluorescence in the scattered light from the biological sample and the effect this may have on the precise measurement of the Stokes parameters and scattering matrix coefficients.

## 2. Experimental configuration

A high-precision spectropolarimeter [4] was used to measure the transmitted or scattered light from a leaf or calibration object. The sample was illuminated with a quartz halogen lamp (Thorlabs QTH10) with an added Lyot depolarizer to ensure only unpolarised light is incident on the sample. A 10 nm narrow band filter (e.g. Thorlabs FB680-10) is placed alternately between the sample and the light source or between the sample and the polarimeter. In the

first case the configuration is optically similar to the laser spectropolarimetry in refs. [3,4,5b] with narrow band illumination. In the second case the white light illuminates the sample and the narrow band filter defines the wavelength of the polarimeter measurement similar to refs [1,2,5a,6]. Differences in the scattered or transmitted light between the two measurements will give an indication of how narrow band and white light polarimetry techniques on leaves and other chlorophyll containing biological material differ.

The experimental configuration for scattering measurements is shown in Fig. 1. The narrow band filters were held in a fixture that allowed precise positioning and orientation to be maintained when moving from between the sample and the polarimeter head (a, after) to between the sample and the illumination source (b, before). Beam stops and shielding were arranged to ensure there was minimal stray light and to confine the illumination to an 8 mm diameter spot on the filter/sample. The stop diameter and the detector apertures combine to a solid angle for scattered light collection of  $\sim 0.02$ sr. The stop positions are indicated in Fig. 1.

Fig. 2 shows the spectrum [Ocean Optics 4000HE] of the input illumination and the transmission curves of the narrow band filters used. For reference a standard solar spectrum is also shown [7].

The spectropolarimeter was optimised for Stokes V and Q measurements and Mueller matrix parameters  $m_{41}$  and  $m_{21}$ , since the incident light is unpolarised. The photoelastic modulator (PEM) was a Hinds I/FS20 and the PMT detectors [Hamamatsu H6779] were connected to a SRS SR830 lock-in amplifier and TEK TPS2024 digital oscilloscope for the ac and dc measurements respectively. A custom LabView Virtual Instrument automated the data collection

E-mail address: [w.e.martin@herts.ac.uk](mailto:w.e.martin@herts.ac.uk)

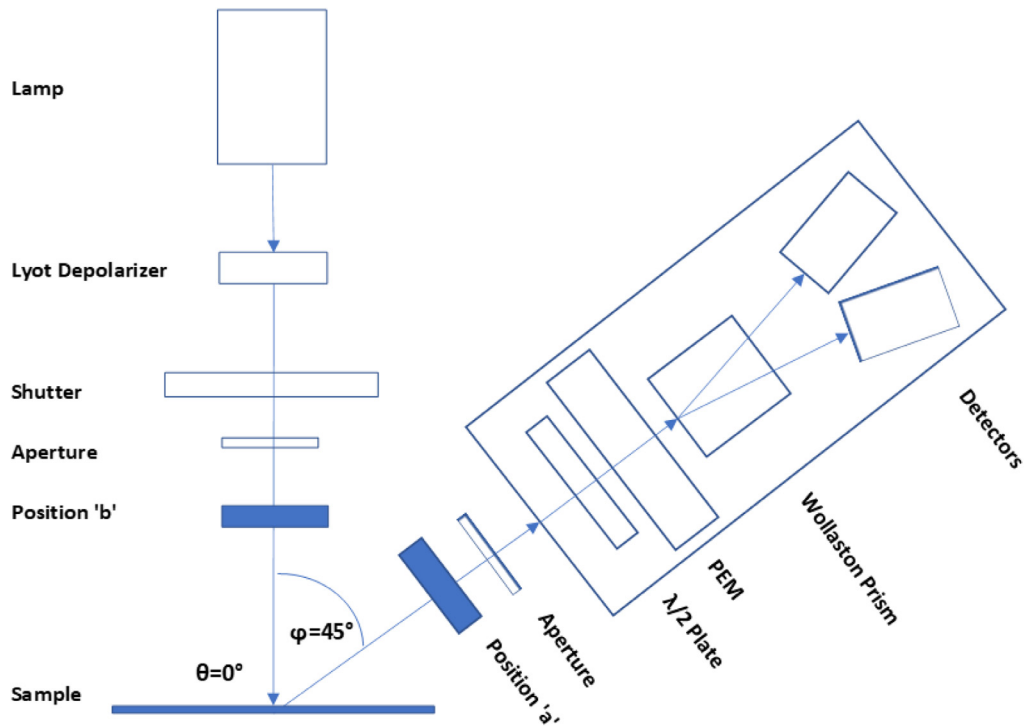


Fig. 1. Instrument diagram. The figure shows the scattering 'R' measurement configuration with the incidence angle  $\theta = 0^\circ$  and the observation angle  $\phi = 45^\circ$ . Positions 'a' and 'b' are the locations of the narrow band filter discussed in the text.

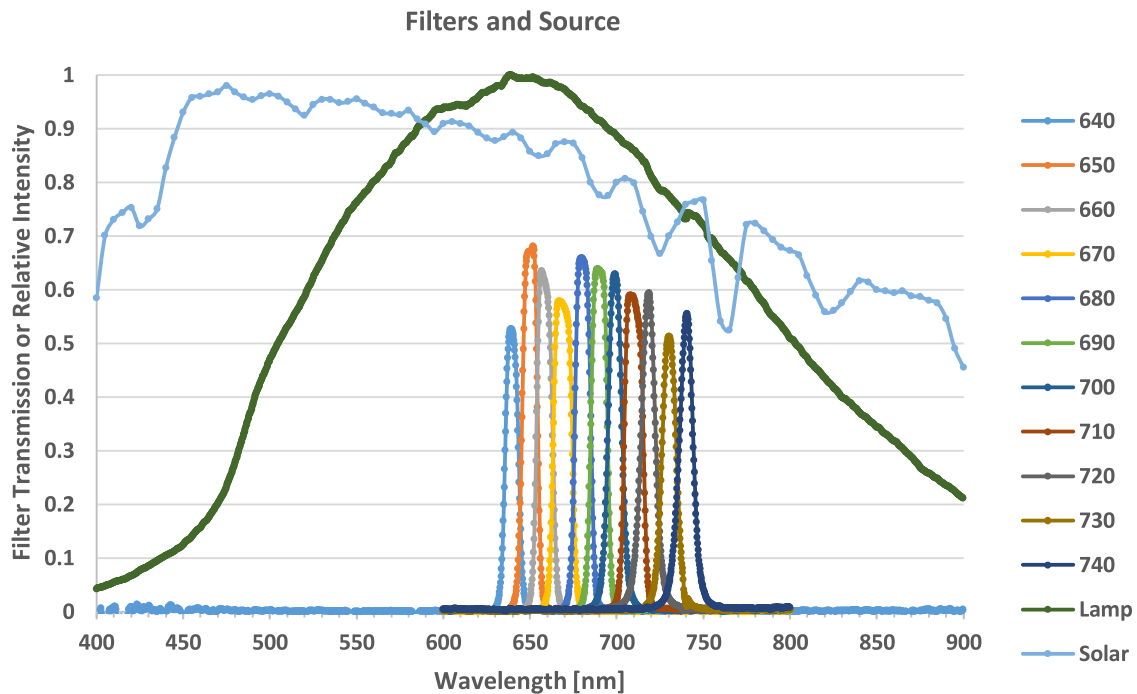


Fig. 2. Source and filter spectra. The 10 nm narrow band filter transmissions are shown with respect to the normalised lamp emission spectrum. Also shown is a typical ground level solar spectrum [7].

process. The samples were illuminated only during the measurements as will be discussed later.

Scattering measurements were taken with the polarimeter at  $45^\circ$  to the beam centre line and with the sample plane normal to the illumination. The incidence angle between the incident light and the surface normal was  $\theta = 0^\circ$ , the observation angle was  $\phi = 45^\circ$ . For transmission measurements  $\theta = 0^\circ$ ,  $\phi = 180^\circ$ .

### 3. Samples and calibration

The incident light source had a residual linear polarization fraction of  $\sim 0.01$  over the lamp emission range and this was reduced to an average of  $\sim 0.001$  over the 640–740 nm measurement range with the use of the Lyot depolarizer.

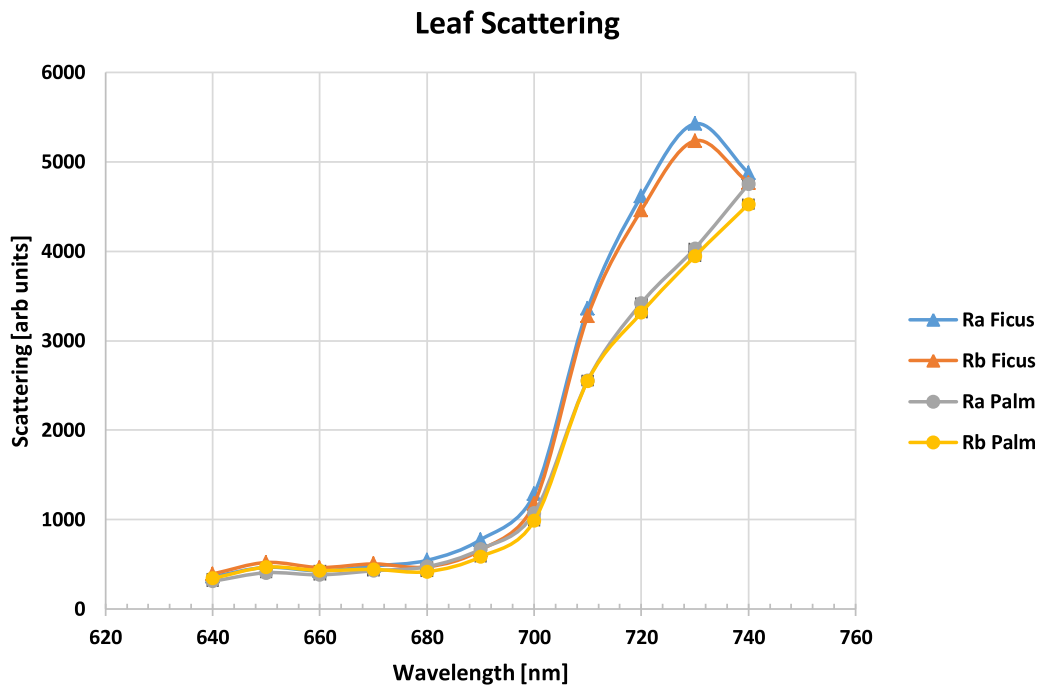


Fig. 3. Leaf scattering measured as total detector signal in the Fig. 1 configuration,  $\theta = 0^\circ$ ,  $\varphi = 45^\circ$ . The  $3\sigma$  error bars are smaller than the data symbols.

A few of the dichroic filters used in the measurements had detectable birefringence ( $\sim 0.02 \lambda$ ). The axial and azimuthal orientation of the filters was rigidly fixed so that no rotation or tilt occurred when the filters were moved between the two measurement positions. Any residual filter birefringence cancels to very low values as will be seen in the data graphs. The approximate average irradiance on the samples for the narrow band illumination was  $3 \times 10^{-4} \text{ W/cm}^2$ ; the irradiance for the white light illumination was  $\sim 3 \times 10^{-2} \text{ W/cm}^2$ .

Calibration of the scattering measurements was accomplished using a Spectralon [15] standard as a uniform Lambertian scatterer. An opal glass diffuser [Edmund 46-167] was used as a consistent reference for the transmission measurements. The latter may have been effected somewhat by residual strain birefringence. The calibration measurements are presented with the leaf measurements.

The experiment is simple in concept but the narrow band and white light intensities are different and it is known that leaves change their optical properties in response to the incident light intensity and the illumination history [8,10-12]. Some data arising from the illumination history will be presented in the Results section.

## 4. Results

The scattered light measurements from the two types of leaves, *Ficus benjamina* and *Chamaedorea elegans*, or 'ficus' and 'palm' respectively are given below. The 'a' values are with the filter after the sample – wide band illumination; the 'b' values are for the filter placed before sample – narrow band illumination.

### 4.1. Total scattering and transmission

The raw data for the total scattered light and transmitted light from the samples is given in Figs. 3 and 4. The 'a' and 'b' measurements are very similar for a given leaf type but the *ficus* and palm leaves have dissimilar scattering and transmission curves. The behaviour of interest begins to emerge when differences between the a and b measurements are calculated. The three sigma error

bars are smaller than the data symbols in these graphs. The curves joining the data points are smooth splines for these and all other graphs and are not physical.

### 4.2. Normalised scattering and transmission differences

The normalised scattering and transmission differences are calculated as follows from the raw measurements:

$$\begin{aligned} ra - rb &= (Ra - Rb)/(Ra + Rb)/2, \\ ta - tb &= (Ta - Tb)/(Ta + Tb)/2 \end{aligned} \quad (1)$$

where  $R_x$  and  $T_x$  are respectively the measured total scattering and transmission intensity measurements from the averaged output of the detectors in Fig. 1.

These values are the difference in the light scattered from the sample or transmitted by the sample at a given wavelength depending on whether the illumination is broad or narrow band. Figs. 5 and 6 below show the result of measurements on the two leaf types and on the calibration samples. Also included in Fig. 5 is a result from a simple model of the scattering to be discussed later. Fig. 5 also shows a scaled fluorescence spectrum derived from a 405 nm laser diode substituted for the lamp illuminating a *Ficus benjamina* leaf in the 'a' configuration. This spectrum is similar to that observed by others [12,13] and uses the same configuration as the scattering measurements.

The scattering, ra-rb, measurements contain spectral features that are similar to a fluorescence spectrum. The ra-rb difference should be principally the difference in fluorescence efficiency between broadband, 'a', and narrow band, 'b' illumination. However, the greater total light flux on the leaves in the 'a' configuration can result in changes in both scattering and fluorescence emission due to adaptation [8,10,11] so the net effect is likely to be complex. Transmission difference measurements are less clear with large differences between the two leaf types and relatively large variations in the opal glass transmission measurements which are reproducible.

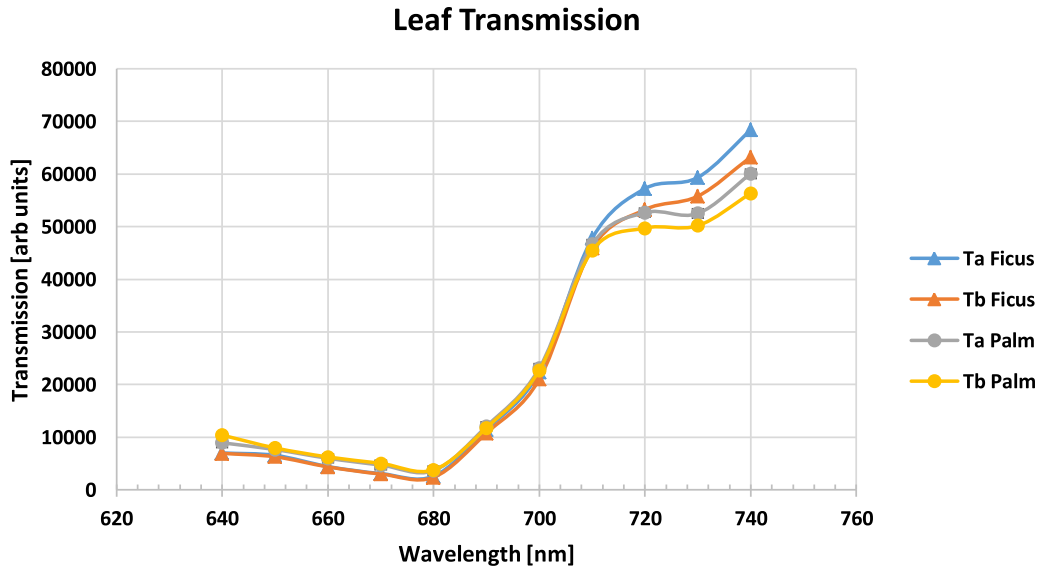


Fig. 4. Leaf transmission measured with  $\theta = 0^\circ$ ,  $\varphi = 180^\circ$ . The  $3\sigma$  error bars are smaller than the data symbols.

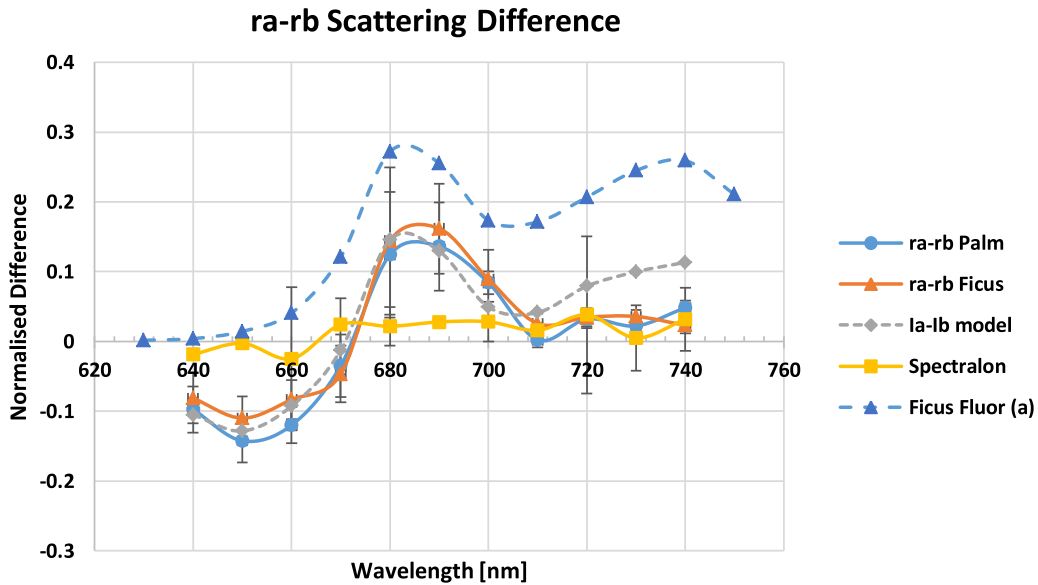


Fig. 5. Normalised scattering differences calculated from the data in Fig. 3 and including the Spectralon scattering standard. The error bars are  $\pm 3\sigma$ . Also included is an la-lb curve derived from the simple model in the Discussion section and a scaled plot of the fluorescence spectrum of *ficus* using a 405 nm laser diode in the 'a' configuration.

#### 4.3. Stokes components and matrix coefficients

The calculation of the Stokes and Mueller Matrix coefficients follows straightforwardly from the modulated signals detected with the lock-in amplifier. With unpolarised illumination the Mueller matrix collapses to a single column vector with only  $m_{11}$ ,  $m_{21}$ ,  $m_{31}$ , and  $m_{41}$  as coefficients. Using this property simplifies the calculations [see Ref 3, Table 1, Eq. (6),  $0^\circ$ ]. The calculations are as follows:

$$\text{Stokes } V = m_{41} = k_1 v(1\omega)\text{rms}/I_{dc}, \quad Q = m_{21} = k_2 v(2\omega)\text{rms}/I_{dc} \quad (2)$$

where  $v(n\omega)$  is the ac voltage from detectors at the appropriate multiple of the PEM modulation frequency  $\omega$ ,  $I_{dc}$  is the dc voltage from the detectors, and  $k_1$  and  $k_2$  are constants incorporating the detection efficiency and conversion from average to rms voltages. For the present instrument these constants are  $k_1 = 0.7342$

and  $k_2 = 0.6106$ .  $V$ ,  $Q$ ,  $m_{41}$ ,  $m_{21}$  are given here in compact form and are the same as  $V/I$ ,  $Q/I$ ,  $m_{41}/m_{11}$ ,  $m_{21}/m_{11}$  in other notations.

The next figures show the  $m_{41}$  and  $m_{21}$  Mueller matrix values which are the same as Stokes  $V$  and  $Q$  respectively. Note that these figures show the magnitude of the coefficients without phases. At  $\sim 710$  nm there is a  $180^\circ$  phase change in both  $m_{41}$  and  $m_{21}$  for both leaf types [3]. These are coefficient values, i.e., normalised to the overall signal levels, and are insensitive to the small differences in overall scattering or transmission levels found in the previous section. The circular scattering values, Stokes  $V$  and  $m_{41}$ , are significantly larger than the linear scattering, Stokes  $Q$  and  $m_{21}$  in the chosen scattering geometry. Fig. 7 also shows an inset with the polarised fluorescence emission components resulting from a 532 nm laser substituted for the lamp in Fig. 1. The *ficus* polarisation coefficients do not have significant wavelength variations or phase changes and this will be discussed in a later section.

The 'b' measurements in Fig. 8 can be compared to the recent extensive Mueller matrix transmission measurements of Patty,

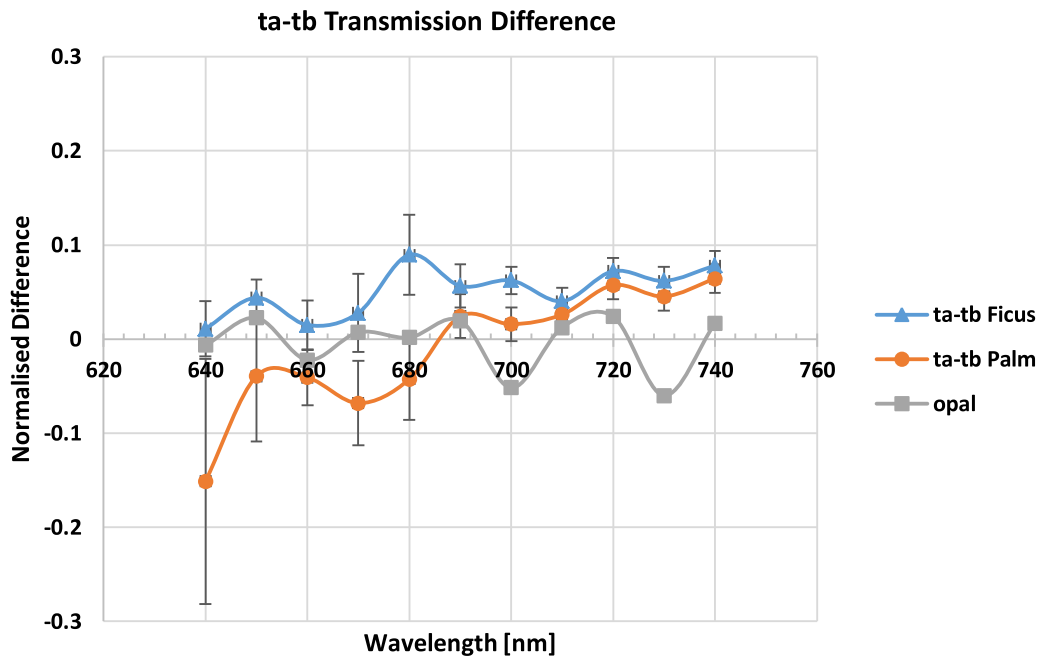


Fig. 6. Normalised transmission differences calculated from the data in Fig. 4. Error bars are  $\pm 3\sigma$ . The large excursions in the opal glass ‘standard’ are reproducible.

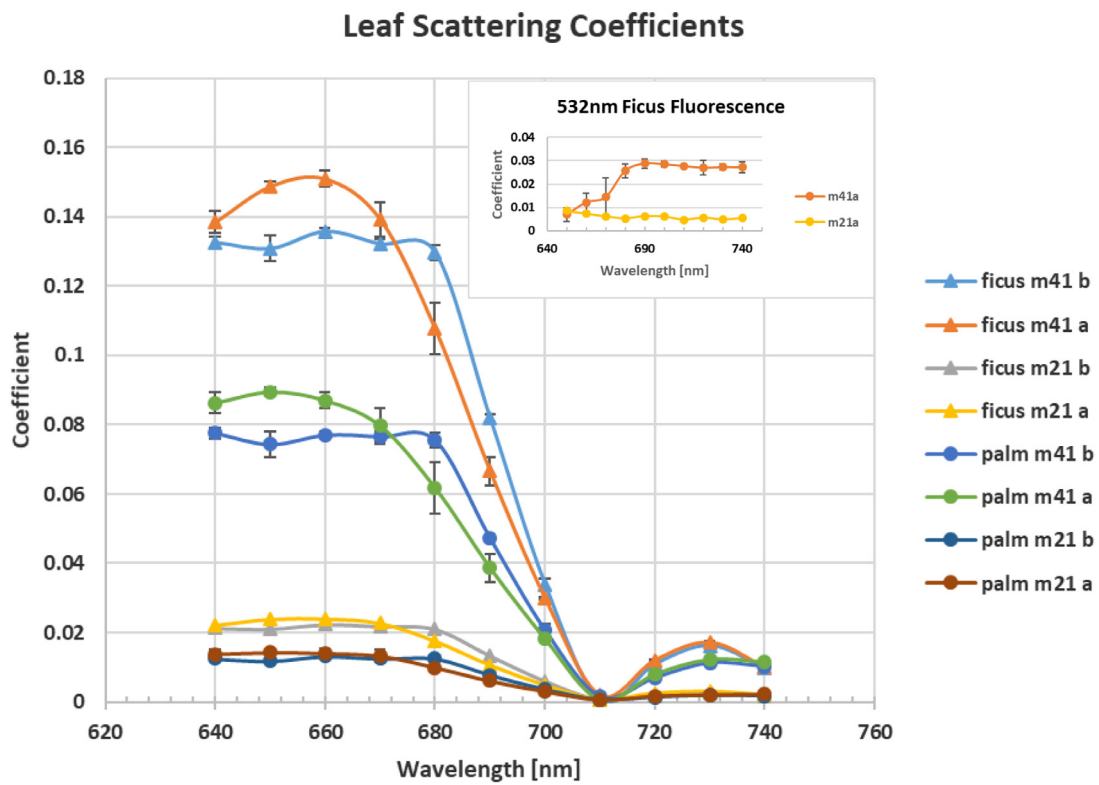


Fig. 7. Mueller matrix scattering coefficients for *ficus* and palm leaves. The ‘b’ measurements are narrow band excitation, the ‘a’ measurements are for broadband illumination.  $\pm 3\sigma$  error bars are visible or are smaller than the data symbols. The small inset shows fluorescence emission coefficients for *ficus* with a 532 nm laser replacing the lamp in Fig. 1 in the ‘a’ configuration.

et al. [5b]. Leaves from maize and maple were measured with an imaging spectropolarimeter able to differentiate between veins and surfaces. Fig. 8 indicates that average transmission coefficients of *ficus* and the thinner palm leaves are different with  $m_{41}$  larger than  $m_{21}$  in both types. In [5b] the magnitudes of the maple and maize coefficients are similar to *ficus* when averaged but the maize  $m_{21}$  coefficients are larger than the  $m_{41}$  for most of the 640–720 nm

range. Fluorescence effects are likely to be small in [5b] but not entirely absent similar to Fig. 8.

Taking the a-b differences, e.g.  $\Delta m_{41} = m_{41a} - m_{41b}$ , as for the total scattering and transmission coefficients gives the following graphs in Figs. 9 and 10. The scattered light polarisation coefficient differences are quite clear and indicate that wide band versus narrow band illumination results in significant differences in

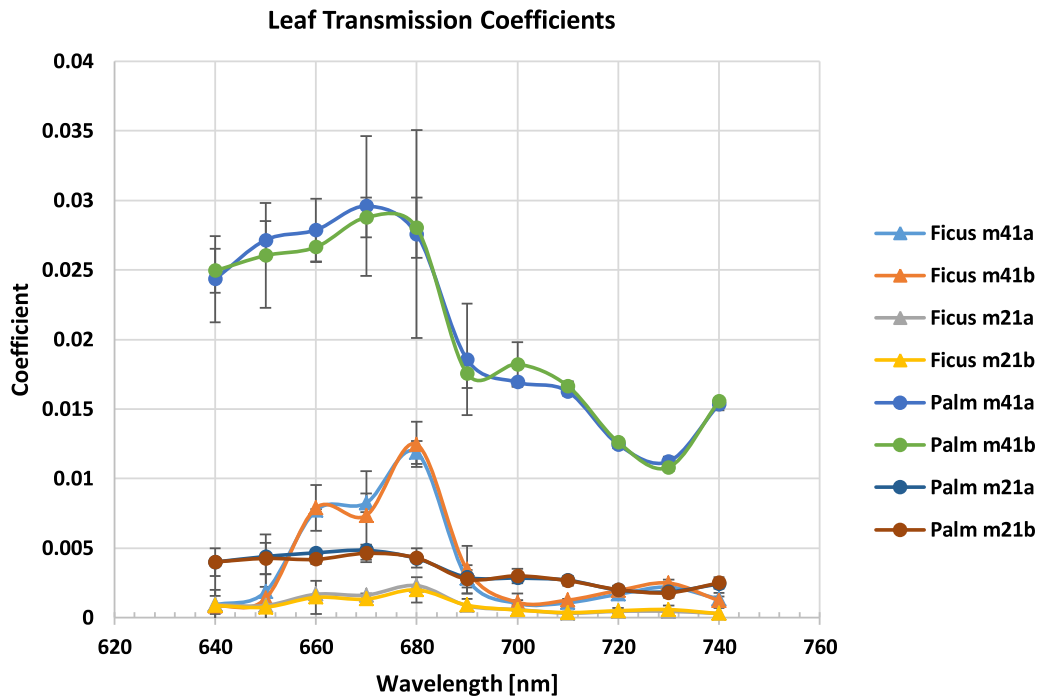


Fig. 8. Mueller matrix transmission coefficients for *ficus* and palm leaves. Error bars are  $\pm 3\sigma$ .

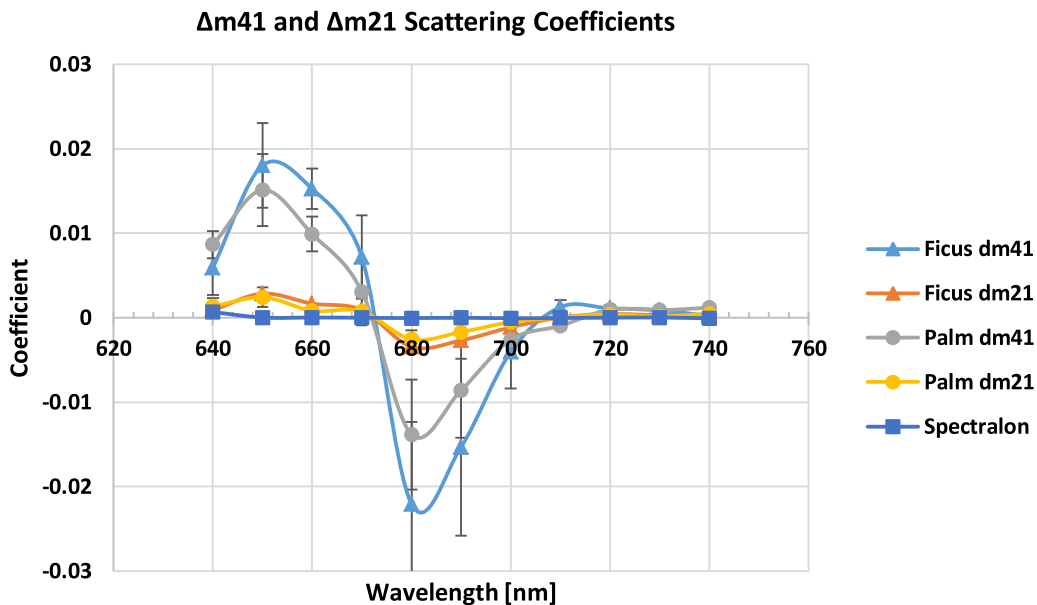


Fig. 9. Differences of the  $m_{41}$  and  $m_{21}$  scattering coefficients for *ficus* and palm leaves. Also shown is the Spectralon scattering standard. Note the changes in sign at  $\sim 670$  nm and  $\sim 710$  nm. Error bars are  $\pm 3\sigma$ .

the scattering coefficients  $m_{41}$  and  $m_{21}$ . Both “unpolarised to circular scattering differences” ( $\Delta m_{41}$ ) and “unpolarised to linear scattering differences” ( $\Delta m_{21}$ ) are present with the linear coefficient differences being an order of magnitude smaller. The transmission coefficient differences are much smaller for both leaves and are relatively free of wavelength dependent features.

#### 4.4. Temporal and illumination variability

A shutter was used to control the exposure of the samples to the illumination source and was opened only during measurements. A typical run of data for a single wavelength consisted of nine sets of five measurements of the Stokes components which

were then averaged and the standard deviation calculated for the total scattering or transmission V and Q components.

Fig. 11 shows a typical total scattering measurement (Ra) illumination history for a palm sample at 670 nm to 690 nm with the filter after the sample, i.e. the sample is illuminated by the full spectrum of the tungsten halogen source during the shutter open times. The temporal changes at shorter and longer wavelengths were much smaller than that at the peak fluorescence of  $\sim 680$  nm. The narrow band (Rb) data shows negligible temporal variations during the illumination periods at all wavelengths.

The light scattered and emitted from the sample has at least two time dependent components, a longer decay time and a shorter recovery time. The longer quenching or decay time con-

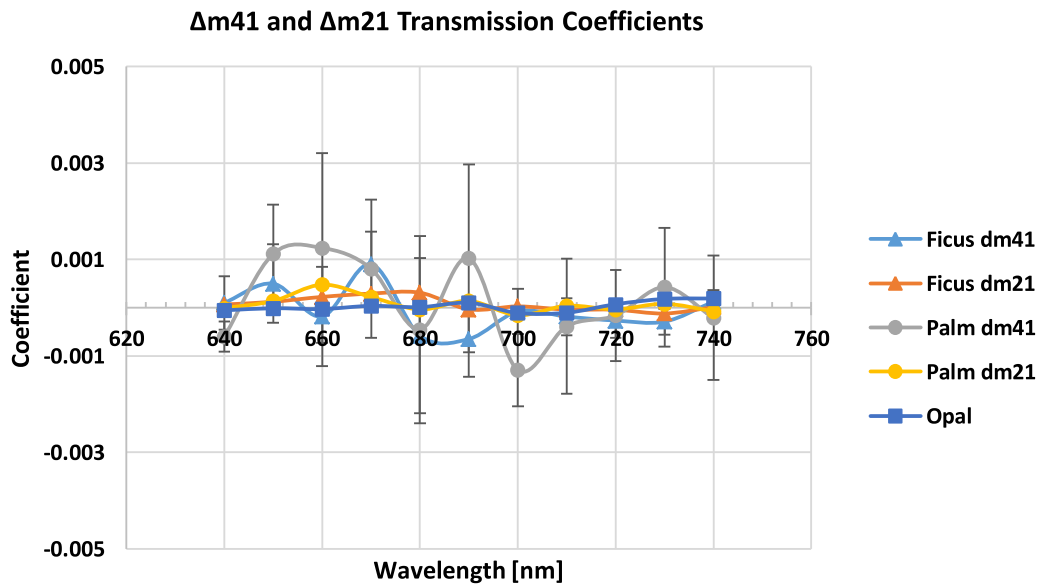


Fig. 10. Differences of the  $m_{41}$  and  $m_{21}$  transmission coefficients for *ficus* and palm leaves. Also shown is the Opal glass transmission standard. Error bars are  $\pm 3\sigma$ .

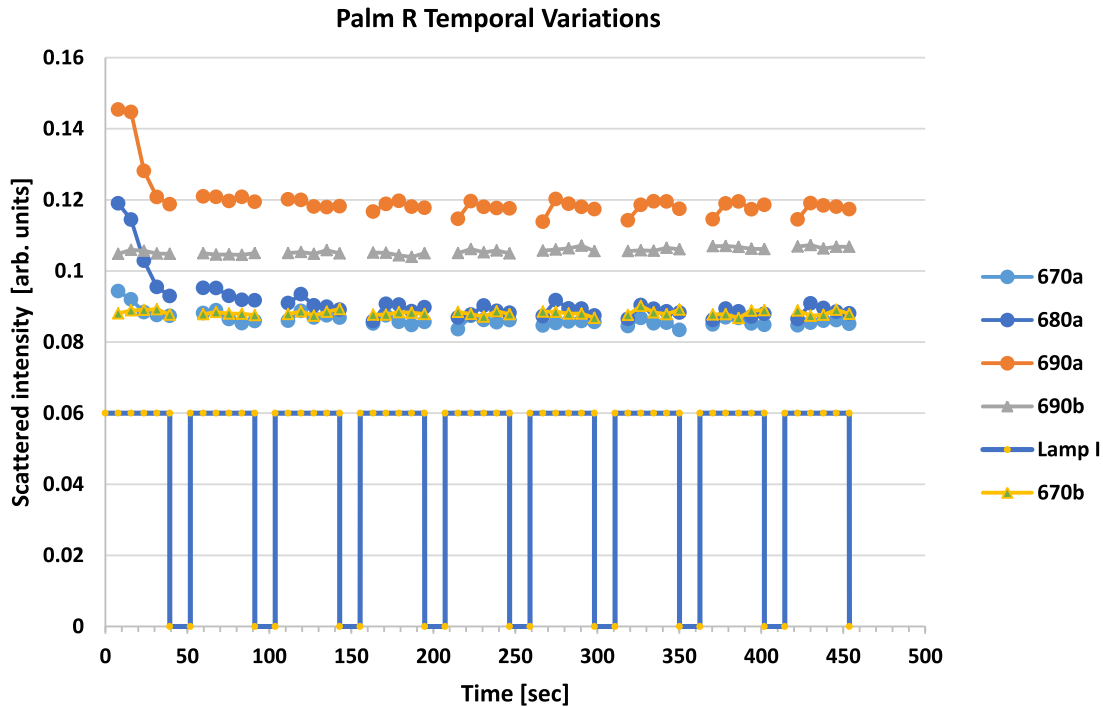


Fig. 11. Temporal variations of scattered light for a palm leaf. These are the individual points in a measurement sequence with the lamp illumination as shown. The broad band illumination ‘a’ measurements show temporal changes during illumination while the ‘b’ measurements do not. Only two ‘b’ sequences are shown at 670 and 690 nm.

stant is approximately 30 s. and the recovery time is approximately 15 s. This behaviour has been studied by many authors [10–12] and the decay times are consistent with quenching and recovery of leaf chlorophyll fluorescence in a dark adapted sample.

### 5. Discussion

There are clear differences between the broad-band illumination (‘a’ or filter after sample) and narrow band illumination (‘b’ or filter before sample) in both scattering and transmission from the leaves. Assuming that broadband illumination will contain the maximum fluorescence, the difference between  $r_a$  and  $r_b$  should reveal the fluorescence spectrum directly. The result of the mea-

surement was that the difference between the ‘a’ and ‘b’ total scattering revealed  $r_a > r_b$  at wavelengths at longer than 680 nm and  $r_a < r_b$  at wavelengths shorter than 680 nm. The difference was about 15% in either case.

A simple model was used to examine this behaviour. The ‘a’ measurement with the filter after the sample is assumed to be of the form

$$I_a(\lambda) = T_f(\lambda) (I_p(\lambda) R(\lambda) + CF(\lambda)) \tag{3}$$

where  $I_a(\lambda)$  is the measured (scattering) intensity,  $T_f(\lambda)$  is the filter transmission,  $I_p(\lambda)$  is the normalised lamp spectrum (see Fig. 2),  $R(\lambda)$  is the leaf reflectivity and  $F(\lambda)$  is the fluorescence intensity.  $C$  is a constant related to fraction of light as fluorescence, i.e., the to-

tal fluorescence emission with broadband illumination at the given unfiltered illumination level. The 'b' measurement is assumed to be of the form

$$I_b(\lambda) = T_f(\lambda) (I_p(\lambda) R(\lambda) + D) \quad (4)$$

where  $I_b(\lambda)$  is the measured (scattering) intensity with the filter before the sample, and  $D$  is a small constant.

$$I_a - I_b = T_f(\lambda) (C F(\lambda) - D) \quad (5)$$

Using the data in Fig. 2 for  $I_p(\lambda)$  and  $T_f(\lambda)$ , the fluorescence data for 405 nm illumination of *ficus* from Fig. 5 for  $F(\lambda)$ , and  $C=0.45$ ,  $D=0.2$  produces the curve of  $I_a-I_b$  in Fig. 5. While the fit to the experimental data in Fig. 5 is not particularly good at longer wavelengths, the major features are captured and the conclusion is that leaf fluorescence accounts for up to 15% of the light from broadband leaf scattering. The principal assumptions are that the leaf reflectivity,  $R(\lambda)$ , is approximately constant with respect to illumination intensity and the fluorescence excitation efficiency is approximately constant with wavelength. Note that the latter assumption implies some fluorescence will be present even with narrow band illumination as long as absorption is present. This means that the a-b measurements here represent a lower bound to the actual fluorescence content of the light detected from broad band illumination. The use of more complex functions for  $D$  involving leaf absorption or reflectivity [13] do not give a significantly better fit to the data. The physical significance of  $D$  can be assigned to a small constant difference in  $R(\lambda)$  between the two different illumination levels of the 'a' and 'b' measurements. This difference is apparent in the data of Fig. 3 but it is not particularly obvious.

The polarisation coefficient measurements are consistent with previous narrow band measurements of leaves with this apparatus [3] which show large circular scattering coefficients at wavelengths shorter than 700 nm, a zero crossing in the scattering coefficient at ~710 nm, and a further rise and fall with a phase reversal at  $\lambda \sim 710$  nm. Differencing the 'a' and 'b' scattering coefficients reveals curves, Fig. 9, showing that both the  $\Delta V$  ( $\Delta m_{41}$ ) and  $\Delta Q$  ( $\Delta m_{21}$ ) scattering (plus fluorescence) are positive for  $\lambda < 670$  nm and negative for  $\lambda > 670$  nm. It is posited that polarised chlorophyll fluorescence is principally responsible for the scattered light  $\Delta V$  ( $\Delta m_{41}$ ) and  $\Delta Q$  ( $\Delta m_{21}$ ) a-b curve shapes.

In a separate measurement in the Fig. 1 apparatus 'a' configuration with 532 nm or 405 nm illumination, excitation that is completely blocked by the filters, the pure fluorescence from a *ficus* leaf in Fig. 3 gives the curves in the inset in Fig. 7 for fluorescence polarisation coefficients. There is no evidence of a polarisation sign change in  $V$  or  $Q$  in this fluorescence signal. These measurements at very high intensity (~0.1 W/cm<sup>2</sup>) revealed differences between the emission spectra with 405 nm and 532 nm illumination and between different samples. Temporal variations with laser illumination are also much larger than seen in Fig. 11 'a' measurements at all wavelengths. See reference [12] for examples of these factors. Further detailed measurements of the fluorescence polarisation emissions versus scattering dependencies are needed at varying illumination levels and on other samples.

The transmission measurement  $t_a-t_b$  differences, Figs. 6, 8, and 10, were less useful because of smaller signal to noise ratios in general and poor performance from the transmission standard. The chlorophyll fluorescence content in leaf transmission light is also subject to self-absorption and the complex absorption and emission properties of the antenna compounds [13,16] as well as additional (multiple) scattering due to internal structures. There is however an indication of transmitted fluorescence in the thinner palm leaves in the form of a negative sign in  $t_a-t_b$  at wavelengths <690 nm in Fig. 6.

Temporal variations in the measured scattering and transmission with broadband illumination point to another consideration in

spectropolarimetric measurements of chlorophyll containing material: Illumination magnitudes and history may be significant to the measurement. The principal effects on the measurements in this paper are seen in Fig. 11 where broadband illumination quenches the 670 nm to 690 nm light from a palm leaf in the initial measurement sequence. Also shown are sequences from the narrow band 'b' measurements at 670 nm and 690 nm for this leaf. Comparing the 690a and 690b sequences, the 'a' broadband illumination quenching results in a ~2% reduction in the average light from the leaf. The 'b' sequence shows no quenching but the scattered light on average is about 12% less (little fluorescence is present). Temporal variations at all other 'b' wavelengths are also unobservable. Although not specifically recorded, repeat measurements after moderate time intervals (20–60 min) on individual leaves indicate the scattered and fluorescence light from the leaf returns to the initial dark adapted level so that no permanent damage is apparent.

## 6. Conclusions

The original premise of this work was that chlorophyll fluorescence would have an effect on the Stokes scattering measured using narrow band light sources [3,4,5b] and broadband sources with monochromators or filters [1,2,5a,6]. This has been shown to be the case in scattered light measurements. Future spectropolarimetric measurements, particularly with sun illuminated vegetation, should carefully consider the contribution of polarised chlorophyll fluorescence to the direct scattering from the leaf surfaces. This will be collection geometry dependent in many experiments, particularly field measurements in remote sensing [5a,6,9,12,17,18]. Partially polarised fluorescence contributes as much as 15% of the measured scattered light between 640 nm and 740 nm in the measurements presented here.

The results in Figs. 5 and 9 indicate that polarised fluorescence is a major component in the variation in scattering coefficients between wide band and narrow band illumination. Previous measurements [3,4] using narrow band illumination have consistently failed to find the 'chiral-like' spectral forms for circular scattering observed in white light experiments [1,2,5a,6]. It is proposed here that a significant portion of chirality signatures previously observed in leaves and bacteria in white light experiments may arise from chlorophyll fluorescence and not direct chiral elastic scattering [14] from chlorophyll containing structures in the biological material. Multiple scattering from structures at or just below the leaf surface will also contribute additional angle dependent circular polarisation components to add to the illumination history dependent polarised fluorescence emissions. The light interaction process is complex to disentangle for all configurations and additional detailed circular polarisation analysis of chlorophyll fluorescence emissions and scattering from in vivo samples will benefit future studies.

The conclusions regarding the sensitivity of spectropolarimetric measurements to chlorophyll chirality for use in remote sensing of exoplanet life should take account of the presence of polarised fluorescence. Fluorescence polarisation is dependent on the chiral properties of chlorophyll and possible chlorophyll analogues and is a strong signature in its own right in scattered light from leaves.

## Declaration of Competing Interests

None.

## Acknowledgements

Thanks to Dr Evelyn Hesse and Prof Hugh Jones for careful reading of several versions of this work and their suggestions

that have made it more readable. The two Reviewers have made very useful suggestions that have improved the presentation. Support from the UK Science and Technology Facilities Council, Grant ST/R0006598/1 is gratefully acknowledged.

### Supplementary material

Supplementary material associated with this article can be found, in the online version, at doi:[10.1016/j.jqsrt.2019.106760](https://doi.org/10.1016/j.jqsrt.2019.106760).

### References

- [1] Sparks WB, Hough JH, Kolokolova L, Germer TA, Chen F, DasSarma S, DasSarma P, Robb FT, Manset N, Reid IN, Macchetto FD. Circular polarization in scattered light as a possible biomarker. *J Quant Spectrosc Radiat Transfer* 2009;110(14–16):1771–9.
- [2] Sparks WB, Hough J, Germer TA, Chen F, DasSarma S, DasSarma P, Robb FT, Manset N, Kolokolova L, Reid N, Macchetto FD. Detection of circular polarization in light scattered from photosynthetic microbes. *Proc Natl Acad Sci* 2009;106(19):7816–21.
- [3] Martin WE, Hesse E, Hough JH, Sparks WB, Cockell CS, Ulanowski Z, Germer TA, Kaye PH. Polarized optical scattering signatures from biological materials. *J Quant Spectrosc Radiat Transfer* 2010;111(16):2444–59.
- [4] Martin WE, Hesse E, Hough JH, Gledhill TM. High-sensitivity stokes spectropolarimetry on cyanobacteria. *J Quant Spectrosc Radiat Transfer* 2016;170:131–41.
- [5a] Patty CL, Visser LJ, Ariese F, Buma WJ, Sparks WB, van Spanning RJ, Röling WF, Snik F. Circular spectropolarimetric sensing of chiral photosystems in decaying leaves. *J Quant Spectrosc Radiat Transfer* 2017;189:303–11.
- [5b] Patty CHL, Luo DA, Snik F, Ariese F, Buma WJ, Kate IL, van Spanning RJM, Sparks WB, Germer TA, Garab G, Kudenov MW. Imaging Linear and circular polarization features in leaves with complete Mueller matrix polarimetry. *BBA-General Subjects* 2018;1862:1350–63.
- [6] Patty, C.H.L., Kate, I.L.T., Buma, W.J., van Spanning, R.J., Steinbach, G., Ariese, F. and Snik, F., 2019. Circular spectropolarimetric sensing of vegetation in the field; possibilities for the remote detection of extraterrestrial life. arXiv:1902.05859.
- [7] <https://redc.nrel.gov/solar//spectra/am1.5/>.
- [8] Maxwell K, Johnson GN. Chlorophyll fluorescence—a practical guide. *J Exp Bot* 2000;51(345):659–68.
- [9] Steinberg IZ. Circular polarization of luminescence: biochemical and biophysical applications. *Annu Rev Biophys Bioeng* 1978;7(1):113–37.
- [10] Baker NR. Chlorophyll fluorescence: a probe of photosynthesis in vivo. *Annu Rev Plant Biol* 2008;59:89–113.
- [11] Krause GH, Weis E. Chlorophyll fluorescence and photosynthesis: the basics. *Annu Rev Plant Biol* 1991;42(1):313–49.
- [12] Agati G. Response of the in vivo chlorophyll fluorescence spectrum to environmental factors and laser excitation wavelength. *Pure Appl Opt* 1998;7(4):797.
- [13] Romero JM, Cordon GB, Lagorio MG. Modeling re-absorption of fluorescence from the leaf to the canopy level. *Remote Sens Environ* 2018;204:138–46.
- [14] Nagdimunov L, Kolokolova L, Mackowski D. Characterization and remote sensing of biological particles using circular polarization. *J Quant Spectrosc Radiat Transfer* 2013;131:59–65.
- [15] <https://www.labsphere.com/>.
- [16] Gantt E. Phycobilisomes. *Annu Rev Plant Physiol* 1981;32(1):327–47.
- [17] Barton CVM, North PRJ. Remote sensing of canopy light use efficiency using the photochemical reflectance index: model and sensitivity analysis. *Remote Sens Environ* 2001;78(3):264–73.
- [18] Moya I, Camenen L, Evain S, Goulas Y, Cerovic ZG, Latouche G, Flexas J, Ounis A. A new instrument for passive remote sensing: 1. measurements of sunlight-induced chlorophyll fluorescence. *Remote Sens Environ* 2004;91(2):186–97.